

# Multi-photon signatures at the Fermilab Tevatron

A.G. Akeroyd<sup>a</sup>, A. Alves<sup>b</sup>, Marco A. Díaz<sup>c</sup>, O. Éboli<sup>b</sup>

*a: Theory Group, KEK, 1-1 Oho, Tsukuba, Japan 305-0801*

*b: Instituto de Física, Universidade de São Paulo, São Paulo, Brazil*

*c: Departamento de Física, Universidad Católica de Chile,  
Avenida Vicuña Mackenna 4860, Santiago, Chile*

## Abstract

Fermiophobic Higgs bosons ( $h_f$ ) exhibiting large branching ratios to two photons can arise in models with two or more scalar doublets and/or triplets. In such models the conventional production mechanisms at hadron colliders, which rely on the  $h_f VV$  coupling ( $V = W, Z$ ), may be rendered ineffective due to severe mixing angle suppression. In this scenario, double  $h_f$  production may proceed via the complementary mechanism  $qq' \rightarrow H^\pm h_f$  with subsequent decay  $H^\pm \rightarrow h_f W^*$ , leading to events with up to 4 photons. We perform a simulation of the detection prospects of  $h_f$  in the multi-photon ( $> 3$ ) channel at the Fermilab Tevatron and show that a sizeable region of the  $(m_{H^\pm}, m_{h_f})$  parameter space can be probed during Run II.

# 1 Introduction

Neutral Higgs bosons with very suppressed couplings to fermions – “fermiophobic Higgs bosons” ( $h_f$ ) [1]– may arise in specific versions of the Two Higgs Doublet Model (2HDM) [2],[3] or in models with Higgs triplets [4]. Such a  $h_f$  would decay dominantly to two photons,  $h_f \rightarrow \gamma\gamma$ , for  $m_{h_f} < 95$  GeV or to two massive gauge bosons,  $h_f \rightarrow VV^{(*)}$ , ( $V = W^\pm, Z$ ) for  $m_{h_f} > 95$  GeV [5, 6]. The large branching ratio (BR) for  $h_f \rightarrow \gamma\gamma$  would provide a very clear experimental signature, and observation of such a particle would strongly constrain the possible choices of the underlying Higgs sector [5, 6, 7, 8, 9, 10, 11].

Experimental searches for  $h_f$  at LEP and the Fermilab Tevatron have been negative so far. Mass limits have been set in a benchmark model which assumes that the coupling  $h_f VV$  has the same strength as the Standard Model (SM) Higgs coupling  $VV\phi^0$ , and that all fermion BRs are exactly zero. Lower bounds of the order  $m_{h_f} \gtrsim 100$  GeV have been obtained by the LEP collaborations OPAL[12], DELPHI[13], ALEPH[14], and L3[15], utilizing the channel  $e^+e^- \rightarrow h_f Z$ ,  $h_f \rightarrow \gamma\gamma$ . At the Tevatron Run I, the limits on  $m_{h_f}$  from the DØ and CDF collaborations are respectively 78.5 GeV [16] and 82 GeV [17] at 95% C.L., using the mechanism  $qq' \rightarrow V^* \rightarrow h_f V$ ,  $h_f \rightarrow \gamma\gamma$ , with the dominant contribution coming from  $V = W^\pm$ . For an integrated luminosity of 2 fb<sup>-1</sup>, Run II will extend the coverage of  $m_{h_f}$  in the benchmark model slightly beyond that of LEP [18],[20]. In addition, Run II will be sensitive to the region  $110 \text{ GeV} < m_{h_f} < 160 \text{ GeV}$  and  $\text{BR}(h_f \rightarrow \gamma\gamma) > 4\%$  which could not be probed at LEP. A preliminary search in the inclusive  $2\gamma + X$  channel has been performed with 190 pb<sup>-1</sup> of Run II data [21].

However, the  $h_f VV$  coupling in a specific model could be suppressed relative to the  $\phi^0 VV$  coupling by a mixing angle, leading to a weakening of the above mass limits. If this suppression were quite severe ( $h_f VV/\phi^0 VV < 0.1$ ) a very light  $h_f$  ( $m_{h_f} \ll 100$  GeV) would have eluded the searches at LEP and the Tevatron Run I in production mechanisms which rely upon the  $h_f VV$  coupling. Therefore it is of interest to consider other production mechanisms for  $h_f$  which may allow observable rates if the  $h_f VV$  coupling is suppressed. Since the couplings  $h_f VV$  and  $h_f VH$  (where  $H$  is another Higgs boson in the model) are complementary, two LEP collaborations, *i.e.* OPAL [12] and DELPHI [13], also searched for fermiophobic Higgs bosons in the channel  $e^+e^- \rightarrow A^0 h_f$ , and ruled out the region  $m_A + m_{h_f} < 160$  GeV. However, a very light  $m_{h_f} < 50$  GeV is still possible if  $m_A$  is sufficiently heavy.

An alternative production mechanism which also depends on the complementary  $h_f VH$  coupling is the process  $qq' \rightarrow H^\pm h_f$  [22], [23]. Such a mechanism is exclusive to a hadron collider, and can offer promising rates at the Tevatron Run II provided that  $H^\pm$  is not too far above its present mass bound  $m_{H^\pm} > 90$  GeV. This alternative experimental signature depends on the decays of  $H^\pm$ . In fermiophobic models the decay  $H^\pm \rightarrow h_f W^{(*)}$  can have a larger BR than the conventional decays  $H^\pm \rightarrow tb, \tau\nu$  [24],[25], which leads to double  $h_f$  production.

In this paper we analyze the inclusive production of multi-photon ( $3\gamma$ 's or  $4\gamma$ 's) final states at the Tevatron RUN II via the mechanism:

$$p\bar{p} \rightarrow h_f H^\pm \rightarrow h_f h_f W^\pm \rightarrow \gamma\gamma\gamma(\gamma) + X .$$

In the 2HDM the multi-photon signature arises in the parameter space  $m_{h_f} \lesssim 90$  GeV,  $m_{H^\pm} \lesssim 200$  GeV, and  $\tan\beta > 1$ . In this region,  $BR(h_f \rightarrow \gamma\gamma) \sim 1$  and  $BR(H^\pm \rightarrow h_f W^{*\pm}) \sim 1$ , leading to a  $4\gamma + \text{leptons}$  or  $\text{jets}$  signature. The multi-photon signature has the added virtue of being extremely clean concerning the background contamination, in contrast to the conventional searches for single  $h_f$  production in the channels  $\gamma\gamma + V$  and  $\gamma\gamma + X$ . In the present work we show that the multi-photon signal can be observed in a large fraction of the  $m_{h_f} \otimes m_{H^\pm}$  plane at the Tevatron RUN II. In fact, at  $3\sigma$  level of statistical significance, the RUN II will be able to exclude Higgs masses up to  $m_{H^\pm} \lesssim 240$  GeV for very light  $m_{h_f}$ , or  $m_{h_f} \lesssim 100$  GeV for  $m_{H^\pm} \approx 100$  GeV.

Our work is organized as follows. In Section 2 we give a brief introduction to fermiophobic Higgs bosons, exhibiting the main decay channels of  $h_f$  and  $H^\pm$ . The possible fermiophobic Higgs production mechanisms and respective signatures are described in Section 3. We present our analyses in Section 4 and Section 5 contains our conclusions.

## 2 Fermiophobic Higgs bosons

In this section we briefly review the properties of  $h_f$ . For a detailed introduction we refer the reader to [6], [9], [10], [11]. Fermiophobia can arise in i) 2HDM (Model I) and ii) Higgs triplets models. In (i) the imposition of a discrete symmetry together with a vanishing mixing angle ensures exact fermiophobia at tree-level. In (ii), gauge invariance forbids any coupling of  $h_f$  to quarks while lepton couplings are strongly constrained by neutrino oscillation data and lepton flavour violation experiments, resulting in approximate fermiophobia at tree-level.

### 2.1 2HDM (Model I)

If  $\Phi_1$  and  $\Phi_2$  are two Higgs  $SU(2)$  doublets with hypercharge  $Y = 1$ , the most general  $SU(2) \times U(1)$  gauge invariant scalar potential is [26]:

$$\begin{aligned}
V = & m_{11}^2 \Phi_1^\dagger \Phi_1 + m_{22}^2 \Phi_2^\dagger \Phi_2 - (m_{12}^2 \Phi_1^\dagger \Phi_2 + h.c.) + \frac{1}{2} \lambda_1 (\Phi_1^\dagger \Phi_1)^2 \\
& + \frac{1}{2} \lambda_2 (\Phi_2^\dagger \Phi_2)^2 + \lambda_3 (\Phi_1^\dagger \Phi_1) (\Phi_2^\dagger \Phi_2) + \lambda_4 (\Phi_1^\dagger \Phi_2) (\Phi_2^\dagger \Phi_1) \\
& + \left\{ \frac{1}{2} \lambda_5 (\Phi_1^\dagger \Phi_2)^2 + [\lambda_6 (\Phi_1^\dagger \Phi_1) + \lambda_7 (\Phi_2^\dagger \Phi_2)] \Phi_1^\dagger \Phi_2 + h.c. \right\} .
\end{aligned} \tag{1}$$

If the discrete symmetry  $\Phi_1 \rightarrow -\Phi_1$  is imposed the couplings  $\lambda_6 = \lambda_7 = 0$ . However, the term proportional to  $m_{12}^2$  can remain as a soft violation of the above discrete symmetry and still ensure that Higgs-mediated tree-level flavour changing neutral currents are absent [3]. Note that the above 2HDM potential contains one more free parameter than those studied in Refs. [10],[11].

The potential in eq. (1) breaks  $SU(2)_L \times U(1)_Y$  down to  $U(1)_{em}$  when the two Higgs doublets acquire vacuum expectation values

$$\langle \Phi_1 \rangle = \frac{1}{\sqrt{2}} \begin{pmatrix} 0 \\ v_1 \end{pmatrix}, \quad \langle \Phi_2 \rangle = \frac{1}{\sqrt{2}} \begin{pmatrix} 0 \\ v_2 \end{pmatrix} \tag{2}$$

which must satisfy the experimental constraint  $m_Z^2 = \frac{1}{2}(g^2 + g'^2)(v_1^2 + v_2^2) \approx (91 \text{ GeV})^2$ . The minimization conditions that define the vacuum expectation values in terms of the parameters of the potential ( $\lambda_6 = \lambda_7 = 0$ ) are

$$\begin{aligned} t_1 &= m_{11}^2 v_1 - m_{12}^2 v_2 + \frac{1}{2} \lambda_1 v_1^3 + \frac{1}{2} (\lambda_3 + \lambda_4 + \lambda_5) v_1 v_2^2 = 0 \\ t_2 &= m_{22}^2 v_2 - m_{12}^2 v_1 + \frac{1}{2} \lambda_2 v_2^3 + \frac{1}{2} (\lambda_3 + \lambda_4 + \lambda_5) v_1^2 v_2 = 0 \end{aligned} \quad (3)$$

from which  $m_{11}^2$  and  $m_{22}^2$  can be solved in favour of  $m_Z^2$  and  $\tan \beta \equiv v_2/v_1$ .

The neutral CP-odd Higgs mass matrix is, after using the minimization conditions,

$$\mathbf{M}_A^2 = \begin{pmatrix} m_{12}^2 t_\beta - \lambda_5 v^2 s_\beta^2 & -m_{12}^2 + \lambda_5 v^2 s_\beta c_\beta \\ -m_{12}^2 + \lambda_5 v^2 s_\beta c_\beta & m_{12}^2/t_\beta - \lambda_5 v^2 c_\beta^2 \end{pmatrix} \quad (4)$$

and is diagonalized by a rotation in an angle  $\beta$ . We define  $s_\beta = \sin \beta$ ,  $c_\beta = \cos \beta$ , and  $t_\beta = \tan \beta$ .  $\mathbf{M}_A^2$  has a zero eigenvalue corresponding to the neutral Goldstone boson while its second eigenvalue is the mass of the physical CP-odd Higgs boson  $A$ ,

$$m_A^2 = \frac{m_{12}^2}{s_\beta c_\beta} - \lambda_5 v^2 \quad (5)$$

with  $v^2 = v_1^2 + v_2^2$ . The charged Higgs mass matrix is given by

$$\mathbf{M}_{H^\pm}^2 = \begin{pmatrix} m_{12}^2 t_\beta - \frac{1}{2} (\lambda_4 + \lambda_5) v^2 s_\beta^2 & -m_{12}^2 + \frac{1}{2} (\lambda_4 + \lambda_5) v^2 s_\beta c_\beta \\ -m_{12}^2 + \frac{1}{2} (\lambda_4 + \lambda_5) v^2 s_\beta c_\beta & m_{12}^2/t_\beta - \frac{1}{2} (\lambda_4 + \lambda_5) v^2 c_\beta^2 \end{pmatrix} \quad (6)$$

which also is diagonalized by a rotation in an angle  $\beta$ . It has a zero eigenvalue corresponding to the charged Goldstone boson, and the charged Higgs mass is

$$m_{H^\pm}^2 = m_A^2 + \frac{1}{2} (\lambda_5 - \lambda_4) v^2. \quad (7)$$

Here we see that the charged and the CP-odd Higgs masses are independent parameters, as opposed to supersymmetry, where the mass squared difference is equal to  $m_W^2$  at tree level.

The neutral CP-even Higgs mass matrix is given by

$$\mathbf{M}_{H^0}^2 = \begin{pmatrix} m_A^2 s_\beta^2 + \lambda_1 v^2 c_\beta^2 & -m_A^2 s_\beta c_\beta + (\lambda_3 + \lambda_4) v^2 s_\beta c_\beta \\ -m_A^2 s_\beta c_\beta + (\lambda_3 + \lambda_4) v^2 s_\beta c_\beta & m_A^2 c_\beta^2 + \lambda_2 v^2 s_\beta^2 \end{pmatrix} \quad (8)$$

and the two eigenvalues are the masses of the neutral CP-even Higgs bosons  $h$  and  $H$ . It is diagonalized by an angle  $\alpha$  defined by

$$\sin 2\alpha = \frac{[-m_A^2 + (\lambda_3 + \lambda_4) v^2] s_{2\beta}}{\sqrt{[m_A^2 c_{2\beta} - \lambda_1 v^2 c_\beta^2 + \lambda_2 v^2 s_\beta^2]^2 + [m_A^2 - (\lambda_3 + \lambda_4) v^2]^2 s_{2\beta}^2}}. \quad (9)$$

Fermiophobia is caused by imposing the mentioned discrete symmetry  $\Phi_1 \rightarrow -\Phi_1$  which forbids  $\Phi_1$  coupling to the fermions. This model is usually called ‘‘Type I’’ [2].

However, fermiophobia is erased due to the mixing in the CP–even neutral Higgs mass matrix, which is diagonalized by the mixing angle  $\alpha$ , when both CP–even eigenstates  $h^0$  and  $H^0$  acquire a coupling to the fermions.

The fermionic couplings of the lightest CP–even Higgs  $h^0$  take the form  $h^0 f \bar{f} \sim \cos \alpha / \sin \beta$ , where  $f$  is any fermion. Small values of  $\cos \alpha$  would strongly suppress the fermionic couplings, and in the limit  $\cos \alpha \rightarrow 0$  the coupling  $h^0 f \bar{f}$  would vanish at tree–level, giving rise to fermiophobia. This is achieved if

$$m_A^2 = (\lambda_3 + \lambda_4)v^2. \quad (10)$$

Despite this extra constraint, the parameters  $m_A$ ,  $m_{H^\pm}$ , and  $\tan \beta$  are still independent parameters in this model.

However, at the one-loop level, Higgs boson couplings to fermions receive contributions from loops involving vector bosons and other Higgs bosons,

$$h_f \text{ --- } \text{loop}(f, \bar{f}) \sim \frac{1}{16\pi^2} (g m_W) \left(\frac{g^2}{8}\right) m_f C_0(m_h^2, 0, 0; 0, m_W^2, m_W^2)$$

where we have naively estimated the contribution of the loop with the Passarino–Veltman function  $C_0$ . To get an order of magnitude of the correction we approximate  $C_0 \sim 1/m_h^2$ , expected in the limit of large Higgs mass, and compare this correction with the tree-level vertex in the SM  $g_{\phi^0 f f} \sim g m_f / 2 m_W$ . We find

$$\frac{\Delta g_{h f f}}{g_{\phi^0 f f}} \sim \frac{g^2}{64\pi^2} \left(\frac{m_W}{m_h}\right)^2. \quad (11)$$

This estimation is also applicable if  $m_h \lesssim m_W$  replacing  $m_h$  by  $m_W$ . This is a very small correction. Nevertheless, we note that the proper renormalization of the  $\phi^0 f \bar{f}$  vertex involves a counterterm that has to be taken into account. It is conventional to define an extreme  $h_f$  in which all BRs to fermions are set to zero. This gives rise to benchmark BRs which are used in the current searches to set limits on  $m_{h_f}$ .

## 2.2 Higgs Triplet Models

Fermiophobia (or partial fermiophobia) can arise for scalar fields in isospin  $I = 1$  triplet representations. Gauge invariance forbids any couplings of the triplet fields ( $\chi$ ) to quarks. For hypercharge  $Y = 2$  triplets, the neutral Higgs field  $\chi^0$  can couple to leptons ( $\nu \bar{\nu}$ ) via the following Yukawa type interaction [27]:<sup>1</sup>

$$h_{ij} \psi_{iL}^T C i \tau_2 \Delta \psi_{jL} + h.c. \quad (12)$$

<sup>1</sup>Note that there is no such interaction for  $Y = 0$  triplets, which are rendered fermiophobic as a consequence of gauge invariance

Here  $h_{ij}(i, j = 1, 2, 3)$  is an arbitrary coupling,  $C$  is the Dirac charge conjugation operator,  $\psi_{iL} = (\nu_i, l_i)_L^T$  is a left-handed lepton doublet, and  $\Delta$  is a  $2 \times 2$  representation of the  $Y = 2$  complex triplet fields:

$$\Delta = \begin{pmatrix} \chi^+/\sqrt{2} & \chi^{++} \\ \chi^0 & -\chi^+/\sqrt{2} \end{pmatrix}. \quad (13)$$

The interaction described in eq. (12) has the virtue of being able to provide neutrino masses and mixings consistent with current neutrino oscillation data, *without* invoking a right-handed neutrino. If the real part of the neutral triplet field  $\chi^{0r}$  acquires a vacuum expectation value (vev)  $\langle \chi^{0r} \rangle = b$ , the following Majorana mass matrix ( $m_{ij}$ ) for neutrinos is generated:

$$m_{ij} = \sqrt{2}h_{ij}b. \quad (14)$$

Neutrino oscillation data constrain the product  $h_{ij}b$ , while  $h_{ij}$  is constrained directly by lepton flavour violating processes involving  $\mu$  and  $\tau$  e.g.  $\mu \rightarrow e\gamma, \mu \rightarrow eee$  [28]. Hence it is clear that  $\chi^0$  is partially fermiophobic, with a small coupling to neutrinos.

We will consider the Higgs Triplet Model (HTM) of reference [4] in which a complex  $Y = 2$  triplet ( $\Delta$ ) and a real  $Y = 0$  triplet ( $\xi^+, \xi^0, \xi^-$ ) are added to the SM Lagrangian. The HTM preserves  $\rho = 1$  at tree-level if the vev's of both the neutral members are equal  $\langle \chi^0 \rangle = \langle \xi^0 \rangle = b$ . Taking the vev of the Higgs doublet  $\langle \Phi^0 \rangle = a$ , one has the following expression for  $m_W$

$$m_W^2 = \frac{1}{4}g^2(a^2 + 8b^2) \equiv \frac{1}{4}g^2v^2 \quad (15)$$

where  $v^2 = 246^2 \text{ GeV}^2$ . It is convenient to define a doublet-triplet mixing angle analogous to  $\tan \beta$  in the 2HDM

$$\sin \theta_H = \left[ \frac{8b^2}{a^2 + 8b^2} \right]^{1/2}. \quad (16)$$

In the HTM the physical Higgs boson mass spectrum is as follows (in the notation of [29])

$$H_5^{\pm\pm}, H_5^\pm, H_5^0, H_3^\pm, H_3^0, H_1^0, H_1^{0'}. \quad (17)$$

The first five scalars are mass eigenstates, while the latter two can mix in general; see below.  $H_1^0$  plays the role of the SM Higgs boson and is composed of the real part of the neutral doublet field. The eigenstate  $H_1^{0'}$  is entirely composed of triplet fields and is given by

$$H_1^{0'} = \frac{1}{\sqrt{3}}(\sqrt{2}\chi^{0r} + \xi^0). \quad (18)$$

From the theoretical point of view, the size of the triplet vev  $b$  is only constrained by the requirement that the doublet vev  $a$  is sufficiently large to allow a perturbative top quark Yukawa coupling. However, experimental constraints on  $\sin \theta_H$  can be obtained by considering the effect of  $H_3^\pm$  on processes such as  $b \rightarrow s\gamma, Z \rightarrow b\bar{b}$  and  $B - \bar{B}$  mixing [30]. Since  $H_3^\pm$  has identical fermionic couplings to that of  $H^\pm$  in the 2HDM (Model I) with the replacement  $\cot \beta \rightarrow \tan \theta_H$ , one can derive the bound  $\sin \theta_H \leq 0.4$ .

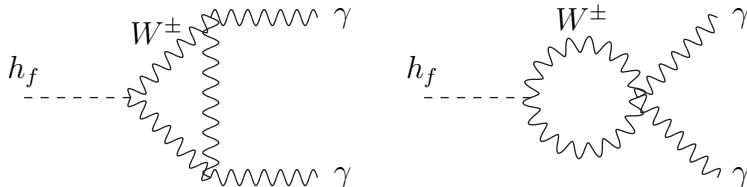
In eq. (18) the  $\chi^{0r}$  component in  $H_1^{0'}$  couples to  $\nu\bar{\nu}$  via the  $h_{ij}$  coupling. One can see from eq. (14) that the decay  $H_1^{0'} \rightarrow \gamma\gamma$ , mediated by  $W$  loops proportional to  $b$ , will dominate over  $H_1^{0'} \rightarrow \nu\bar{\nu}$  if  $b$  is of the order of a few GeV. Thus  $H_1^{0'}$  is a candidate for a  $h_f$ , with  $\text{BR}(H_1^{0'} \rightarrow \gamma\gamma)$  essentially equal to that of the benchmark  $h_f$  model. However, in general  $H_1^0$  and  $H_1^{0'}$  mix through the following mass matrix written in the  $(H_1^0, H_1^{0'})$  basis [29]

$$\mathcal{M} = \begin{pmatrix} 8c_H^2(\lambda_1 + \lambda_3) & 2\sqrt{6}s_H c_H \lambda_3 \\ 2\sqrt{6}s_H c_H \lambda_3 & 3s_H^2(\lambda_2 + \lambda_3) \end{pmatrix} v^2. \quad (19)$$

Here  $\lambda_i$  are dimensionless quartic couplings in the Higgs potential and  $s_H = \sin\theta_H, c_H = \cos\theta_H$ . The assumption that the  $\lambda_i$  couplings are roughly the same order of magnitude together with the imposition of the bound  $s_H < 0.4$  results in very small mixing [31]. Moreover,  $H_1^{0'}$  would be the lightest Higgs boson in the HTM limit of small  $s_H$ , as stressed in [32]. In this paper we will study the production process  $qq' \rightarrow H_3^\pm H_1^{0'}$ , assuming that  $H_1^{0'}$  is a fermiophobic Higgs with BRs equivalent to the benchmark  $h_f$  model.

### 2.3 Fermiophobic Higgs boson branching ratios

For the sake of illustration, we depict in Fig. 1 the branching ratios of a fermiophobic Higgs boson  $h_f$  into  $VV$  where  $V$  can be either a  $W, Z$  or  $\gamma$ . In this figure we assumed that the  $h_f$  couplings to fermions are absent and that  $h_f \rightarrow \gamma\gamma$  is mediated solely by a  $W$  boson loop,



giving rise to the following  $h_f$  branching ratio into two photons,

$$\Gamma(h_f \rightarrow \gamma\gamma) = \frac{\alpha^2 g^2}{1024\pi^3} \frac{m_{h_f}^3}{m_W^2} |F_1 \cos\beta|^2 \quad (20)$$

with  $F_1 = F_1(\tau)$ ,  $\tau = 4m_W^2/m_{h_f}^2$ , a function given in [3]. We remind the reader that the  $h_f WW$  coupling normalized to the SM  $\phi_0 WW$  coupling satisfies  $\sin(\beta - \alpha) \rightarrow \cos\beta$  in the fermiophobic limit.

This gives rise to benchmark BRs which are used in the ongoing searches to derive mass limits on  $m_{h_f}$ . In practice,  $h_f \rightarrow \gamma\gamma$  can also be mediated by charged scalar loops:  $H^\pm$  in the 2HDM [10],[11] and  $H_3^\pm, H_5^\pm, H_5^{\pm\pm}$  in the HTM [33]. Although such contributions are suppressed relative to the  $W$  loops by a phase space factor, they can be important if the mixing angle suppression for the  $h_f WW$  coupling ( $\cos\beta$ ) is quite severe *i.e.* the scenario of interest in this paper. In our numerical analysis we will assume the benchmark BRs

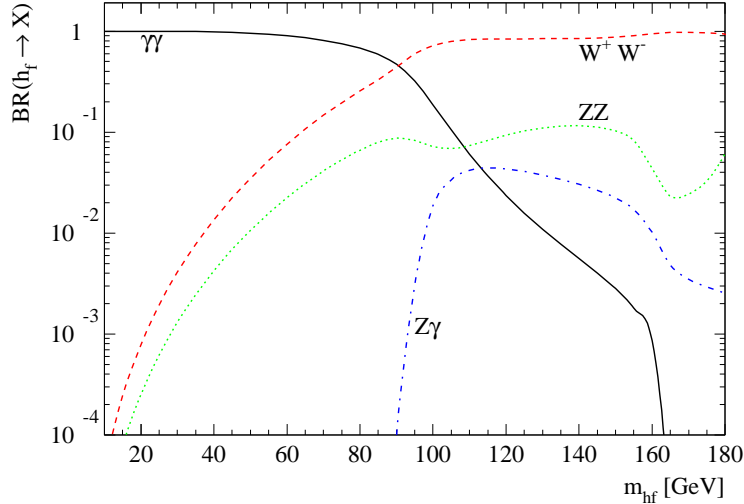


Figure 1: Branching ratios of the largest decay modes of a fermiophobic Higgs boson assuming exact fermiophobia at tree-level. The branching ratio into  $\gamma\gamma$  equals the  $W^*W^*$  mode for  $m_{h_f} \approx 90$  GeV and drops to 20% for  $m_{h_f} = 100$  GeV.

given in Fig. 1. One can see from the figure that the loop induced decay mode  $h_f \rightarrow \gamma\gamma$  is dominant for  $m_{h_f} \lesssim 95$  GeV and drops below 0.1% for  $h_f$  masses above 150 GeV. On the other hand, the decay channel  $h_f \rightarrow W^*W^*$  dominates for  $m_{h_f} \gtrsim 95$  GeV, being close to 100% until the threshold for  $h_f$  decay into two real  $Z$ 's is reached.

## 2.4 The decay $H^\pm \rightarrow h_f W^*$

The experimental signature of the process  $qq' \rightarrow H^\pm h_f$  depends on the decay modes of  $H^\pm$ . If  $H^\pm$  decays to two fermions then the signal would be of the type  $\gamma\gamma + X$ , which is essentially the same as that assumed in the inclusive searches. However, crucial to our analysis is the fact that the decay  $H^\pm \rightarrow h_f W^*$  may have a very large BR [24] in the 2HDM (Model I). This is because the decay width to the fermions ( $H^\pm \rightarrow f'\bar{f}$ ) scales as  $1/\tan^2\beta$ . Similar behaviour occurs in the HTM [25] for the decay  $H_3^\pm \rightarrow H_1^{0'}W^*$  with the replacement  $1/\tan^2\beta \rightarrow \tan^2\theta_H$ . Thus in the region of  $\tan\beta > 10$  (or small  $\sin\theta_H$ ) the fermionic decays of  $H^\pm$  are depleted. This enables the decay  $H^\pm \rightarrow h_f W^*$  ( $H_3^\pm \rightarrow H_1^{0'}W^*$ ) to become the dominant channel *even if* the mass difference  $m_{H^\pm} - m_{h_f}$  is much less than  $m_W$ . In Fig. 2 we show the branching ratios of the charged Higgs boson into fermions and  $h_f W^*$  as a function of  $M_{H^\pm}$  for several values of  $\tan\beta$  and  $m_{h_f}$ . From the right panels we see that in the large  $\tan\beta$  regime the fermionic decays are indeed suppressed. Moreover, we also see that for light fermiophobic Higgs bosons, where a  $W$  boson can be produced on its mass shell, the decay  $H^\pm \rightarrow W^\pm h_f$  is essentially 100% for any  $\tan\beta$ . On the other hand, for heavier fermiophobic Higgs bosons, the fermionic decays can be the preferred decay channels mainly for small  $\tan\beta$ .

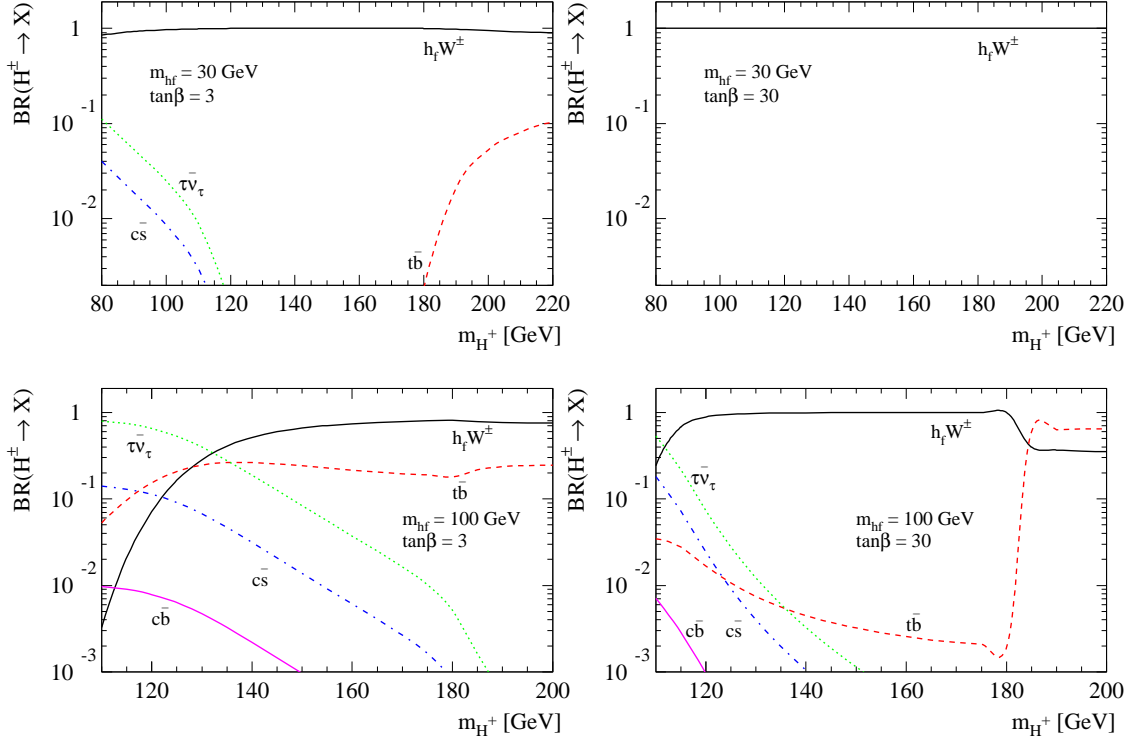


Figure 2: The charged Higgs boson branching ratios into fermions  $\tau\nu_\tau$  (green/dotted),  $tb$  (red/dashed),  $cs$  (blue/dot-dashed), and  $cb$  (magenta/solid), and  $W^*h_f$  (black/solid) as a function of the charged Higgs boson mass for two different  $\tan\beta$  and fermiophobic Higgs mass values.

### 3 Phenomenology of $h_f$ at hadron colliders

#### 3.1 $h_f$ production via the $VVh_f$ coupling

Current searches at the Tevatron assume that production of  $h_f$  proceeds via the  $VVh_f$  coupling ( $V = W, Z$ ) that originates from the kinetic part of the Lagrangian. Run I searches utilized the process  $qq' \rightarrow Vh_f$  giving a signature of a  $\gamma\gamma$  and a vector boson [16],[17]. The preliminary Run II search is for inclusive  $\gamma\gamma$  [21] and is therefore sensitive to both  $qq' \rightarrow Vh_f$  and the subdominant vector boson fusion  $qq' \rightarrow h_f qq$ ; see [18]. Note that  $gg \rightarrow h_f$  via a fermion loop does not contribute to  $h_f$  production.

In the 2HDM (Model I) the strength of the  $VVh_f$  coupling relative to the SM coupling  $VV\phi^0$  is given by

$$VVh_f \propto \frac{1}{\sqrt{1 + \tan^2 \beta}}. \quad (21)$$

Hence the production mechanism  $qq \rightarrow V^* \rightarrow Vh_f$  can be rendered completely ineffective for  $\tan\beta > 10$ . In the HTM the fermiophobic Higgs boson has a coupling size relative to

$VV\phi^0$  given by

$$VVH_1^{0'} \propto \frac{2\sqrt{2}}{\sqrt{3}} s_H . \quad (22)$$

In direct analogy to the large  $\tan\beta$  case of the 2HDM (Model I), a small  $s_H$  would suppress the coupling  $VVH_1^{0'}$  and consequently deplete the  $h_f V$  production. Hence it is of concern to consider other production mechanisms which are unsuppressed in the above scenario.

### 3.2 Associated $h_f$ production with $H^\pm$ and the multi-photon signature

The production mechanism  $qq' \rightarrow H^\pm h_f$  is complementary to that of  $qq' \rightarrow Vh_f$ . This can be seen immediately from the explicit expressions for the couplings. In the 2HDM (Model I) one has

$$VH^\pm h_f \propto \frac{\tan\beta}{\sqrt{1+\tan^2\beta}} , \quad (23)$$

while in the HTM

$$VH^\pm H_1^{0'} \propto \frac{2\sqrt{2}}{\sqrt{3}} c_H . \quad (24)$$

Hence the above couplings are unsuppressed in the region of the parameter space where the standard production mechanism  $qq' \rightarrow Vh_f$  becomes ineffective. The larger coefficient for the  $VH_3^\pm H_1^{0'}$  coupling is a consequence of the quantum number ( $I, Y$ ) assignments in the HTM.

To date complementary mechanisms have not been considered in the direct fermiophobic Higgs searches at the Tevatron. As emphasized in [22], [23] a more complete search strategy for  $h_f$  at hadron colliders must include such production processes in order to probe the scenario of fermiophobic Higgs bosons with a suppressed coupling  $h_f VV$ . In the HTM one expects  $H_1^{0'}$  to be the lightest Higgs boson for small  $\sin\theta_H$ , which further motivates a search in the complementary channel  $qq' \rightarrow H_3^\pm H_1^{0'}$ .

The experimental signature arising from the complementary mechanism  $qq' \rightarrow H^\pm h_f$  depends on the  $H^\pm$  decay channel. In a large fraction of the parameter space where the complementary mechanism  $qq' \rightarrow H^\pm h_f$  is important, the  $H^\pm$  decay is dominated by  $H^\pm \rightarrow h_f W^*$ . Consequently, this scenario would give rise to double  $h_f$  production, with subsequent decay of  $h_f h_f \rightarrow \gamma\gamma\gamma\gamma, VV\gamma\gamma$  and  $VVVV$ . For light  $h_f$  ( $m_{h_f} \lesssim 90$  GeV), the signal  $\gamma\gamma\gamma\gamma$  would dominate, as discussed in [24] at LEP, in [22] for the Tevatron Run II and [23] at the LHC and a Linear Collider. More specifically, the multi-photon signature arises in the portion of the parameters space where  $m_{h_f} \lesssim 90$  GeV,  $m_{H^\pm} \lesssim 200$  GeV, and  $\tan\beta > 1$  in the 2HDM Model I framework. In that region,  $BR(h_f \rightarrow \gamma\gamma) \sim 1$  and  $BR(H^\pm \rightarrow h_f W^{*\pm}) \sim 1$  as well, leading to a  $4\gamma + \text{leptons}$  or jets signature.

As explained in [22], processes other than  $qq' \rightarrow H^\pm h_f$  could give rise to a  $4\gamma + X$  signal. One such mechanism is  $q\bar{q} \rightarrow A^0 h_f$ , where  $A^0$  is the heavy neutral pseudoscalar decaying  $A^0 \rightarrow h_f Z^*$ . However, LEP already searched for  $e^+e^- \rightarrow h_f A^0$  and set the bound  $m_{h_f} + m_{A^0} > 160$  GeV [12]. Thus any contribution from  $qq \rightarrow A^0 h_f$  will be phase space

suppressed relative to that originating from  $qq' \rightarrow H^\pm h_f$ . A similar argument applies to the production of a pair of charged Higgs bosons and its subsequent decay into  $h_f V^*$  pairs, *i.e.*  $q\bar{q} \rightarrow Z^*, \gamma^* \rightarrow H^+ H^- \rightarrow h_f h_f W^+ W^-$  which is phase space suppressed at Tevatron energies ( $2m_{H^\pm} > 180$  GeV from direct  $H^\pm$  searches). In the minimal supersymmetric model the total rates for  $H^+ H^-$  production are enhanced in the large  $\tan \beta$  regime through the Yukawa couplings of Higgs bosons to bottom quarks [34], however in the 2HDM Model I and HTM, these Yukawa couplings are suppressed. The LHC would probably have much better prospects in these additional channels if all the above pair production mechanisms were combined with the  $H^\pm h_f$  associated production in a fully inclusive multi-photon search. Since our analysis for the Tevatron we will focus on  $qq' \rightarrow H^\pm h_f$ , which provides the best search potential for the very light  $h_f$  region because the phase space constraint ( $m_{H^\pm} + m_{h_f} > 100$  GeV) is the least restrictive of the Higgs pair production mechanisms.

## 4 Multi-photon signal analyses

We now present our analysis for the inclusive production of multi-photon final states which may or may not be accompanied by extra leptons and/or jets, *i.e.* the reaction

$$p\bar{p} \rightarrow h_f H^\pm \rightarrow h_f h_f W^\pm \rightarrow \gamma\gamma\gamma\gamma + X$$

at the Tevatron Run II. We focus our attention on two inclusive final states; i) at least three photons ( $> 3\gamma$ ) and ii) four photons ( $4\gamma$ ). Only the “1-prong” tau lepton decays were considered.

In our analysis we evaluated the signal and standard model backgrounds at the parton level. We calculated the full matrix elements using the helicity formalism with the help of MadEvent [35]. We employed CTEQ6L1 parton distributions functions [36] evaluated at the factorization scale  $Q_F = \sqrt{\hat{s}}$ , where  $\sqrt{\hat{s}}$  is the partonic center-of-mass energy. Although QCD corrections increase the tree-level cross section by a factor of around 1.3 [37], we shall present results using the tree-level cross sections only. Moreover we included momenta smearing effects as given in [16], [38] and a detection efficiency of 85% per photon.

We present in Fig. 3 the total signal cross section times the branching ratios of  $H^\pm \rightarrow h_f W^\pm$  and  $h_f \rightarrow \gamma\gamma$  for the complementary process  $qq' \rightarrow H^\pm h_f$ ; these results were obtained without cuts and detection efficiencies. In the left (right) panel we present the  $4\gamma$  production cross section before cuts as a function of  $m_{h_f}$  for three different values of  $m_{H^\pm}$  and  $\tan \beta = 3$  (30). In the left panel, where  $\tan \beta = 3$ , the upper curve ( $m_{H^\pm} = 100$  GeV) shows the strongest effect of the phase space suppression of the decay  $H^\pm \rightarrow W^* h_f$  for  $m_{h_f} \gtrsim 60$  GeV. This cross section reduction can be partially compensated by the increase in  $\tan \beta$  as shown in the right panel. From the figure it is evident that this process will produce a large number of events before cuts over a large fraction of the parameter space.

Potential SM backgrounds for the multi-photon signature of fermiophobic Higgs bosons are: i) the three and four photon production  $p\bar{p} \rightarrow \gamma\gamma\gamma(\gamma)$ , ii) three photons and a  $W$

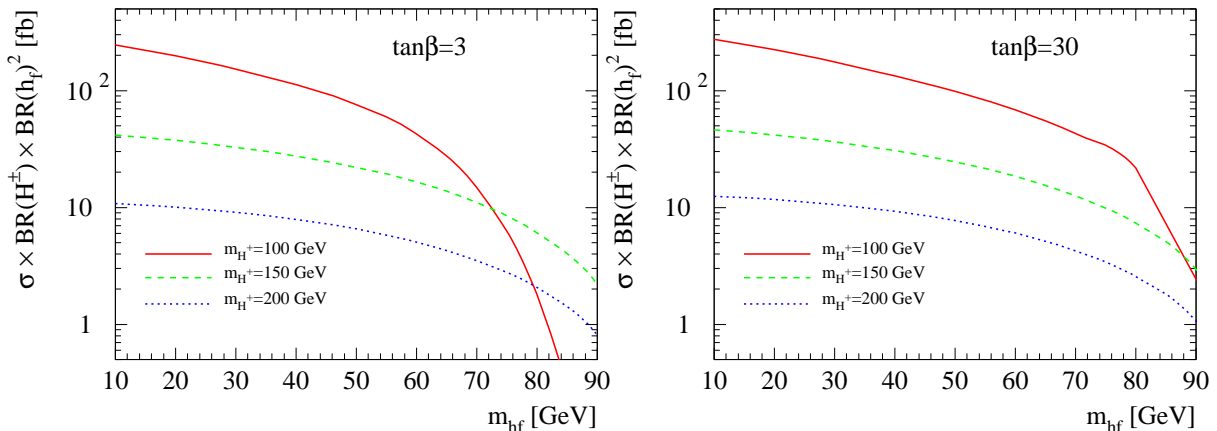


Figure 3: Total production cross sections times branching ratios of  $h_f \rightarrow \gamma\gamma$  and  $H^\pm \rightarrow W^\pm h_f$  for  $p\bar{p} \rightarrow h_f H^\pm \rightarrow h_f h_f + W^\pm \rightarrow \gamma\gamma\gamma\gamma + W^\pm$  before cuts at the Tevatron Run II in femtobarns. The values of  $\tan\beta$  and  $m_{H^\pm}$  are as indicated in the figure.

production  $p\bar{p} \rightarrow \gamma\gamma\gamma W$ , and iii) the associated production of two or three photons and a jet where the latter is misidentified as a photon  $p\bar{p} \rightarrow \gamma\gamma(\gamma)j(\rightarrow \gamma + X)$ . We verified that after cuts and taking into account a  $P(j \rightarrow \gamma) = 4 \times 10^{-4}$  [38] photon misidentification probability the total SM background amounts to 3.8 events for an integrated luminosity of  $2 \text{ fb}^{-1}$ . Therefore the complementary process for the fermiophobic Higgs search has the great advantage of being extremely clean for a large portion of the 2HDM and HTM parameter space. In contrast, the ongoing search for inclusive  $\gamma\gamma + X$  [21] suffers from a sizeable background originating from QCD jets faking photons. For the exclusive channel ( $\gamma\gamma + V$ ) the background is considerably smaller but still not negligible [16],[17].

#### 4.1 Searches at the Tevatron Run II

The multi-photon topology is privileged concerning the level of background, which is small in the SM after mild cuts. Consequently, we imposed a minimum set of cuts on the final state particles, in order to guarantee their identification and isolation. Further studies could optimize the search strategy. We required the events to possess central photons with enough transverse energy to assure their proper identification

$$E_T^\gamma > 15 \text{ GeV} \quad , \quad |\eta^\gamma| < 1.0 \quad , \quad (25)$$

and isolated from the other particles in the final state ( $X = \text{charged lepton or jet}$ ) with a transverse energy in excess of 5 GeV

$$\Delta R_{\gamma\gamma} > 0.4 \quad , \quad \Delta R_{\gamma X} > 0.4 \quad . \quad (26)$$

Notice that the high  $p_T$  central photons is enough to guarantee the trigger of these events [38]. These cuts are very effective against the backgrounds from continuous  $\gamma\gamma\gamma + X$

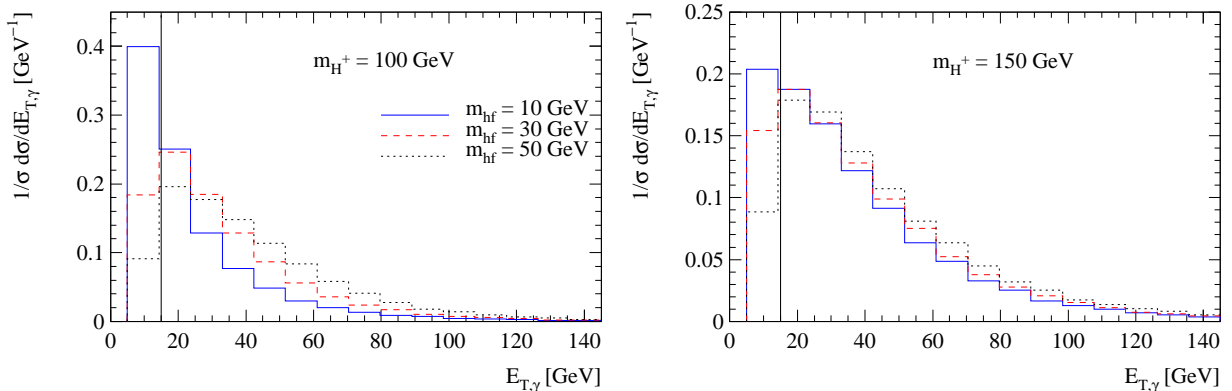


Figure 4: Normalized transverse energy distributions (in GeV) of photons for two different charged Higgs boson masses and three different fermiophobic Higgs masses. The vertical solid lines indicate the  $E_T^\gamma$  cut in eq. (25).

production which occur mainly through photon and gluon bremsstrahlung emission from initial and/or final state quarks, and gluon splitting to collinear quarks. We have checked that  $4\gamma + X$  topologies give a negligible contribution after imposing the cuts.

In order to understand the effect of these cuts on the signal we studied some kinematical distributions. We present in Fig. 4 the normalized transverse energy distribution of the final state photons for several values of Higgs masses and  $\tan\beta = 30$ . As one can see, the  $E_T^\gamma$  spectrum peaks around  $\lesssim m_{h_f}/2$  and the spectrum at low  $E_T^\gamma$  decreases as the fermiophobic Higgs becomes heavier. We can also learn that the  $E_T^\gamma$  distribution becomes harder as the charged Higgs mass increases. Thus, the transverse energy cut in eq. (25) attenuates more the light fermiophobic Higgs signal.

Figure 5 contains the photon rapidity distribution for the same parameters used in Fig. 4. The rapidity distribution of the photons stemming from the fermiophobic Higgs decay peaks around zero. However, there is a sizeable contribution from high rapidity photons. For heavier charged Higgs bosons the rapidity distribution is more central. The hardest cut that we applied is the requirement that the absolute value of the photon rapidity be smaller than unity, and its effect is rather insensitive to the neutral Higgs mass. On the other hand, the separation cuts in eq. (26) have little effect on the signal cross section as shown in Fig. 6, with perhaps the exception of very small fermiophobic Higgs masses. Notice that we did not introduce any cut on the photon–photon invariant masses. Certainly if a signal is observed the photon pair invariant mass will display a clear peak at  $m_{h_f}$  even after adding all the possible photon pair combinations and backgrounds; see Fig. 7.

We display in Figure 8 the region in the plane  $m_{H^\pm} \otimes m_{h_f}$  where at least a  $3\sigma$  signal can be observed, exhibiting three or more photons, in the framework of the 2HDM Model

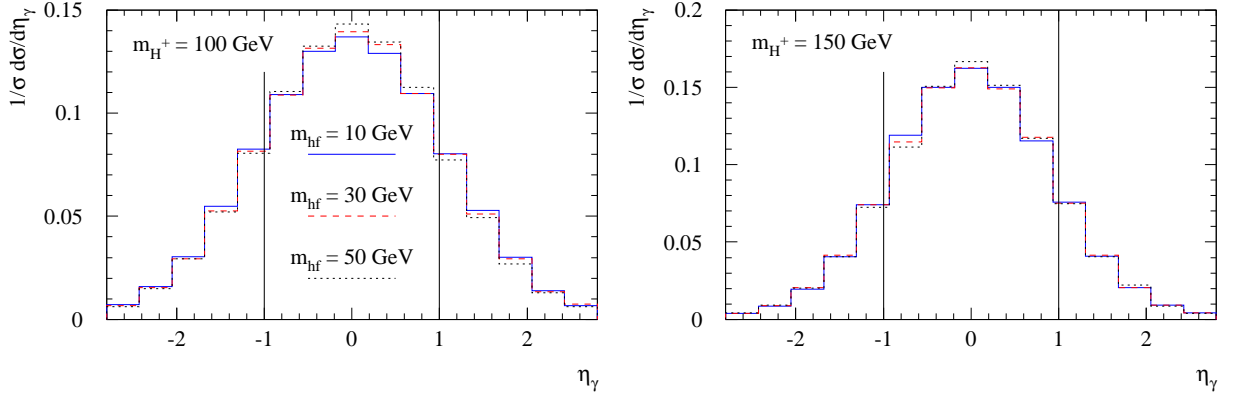


Figure 5: Normalized rapidity distributions of photons for two different charged Higgs boson masses and three different fermiophobic Higgs masses. The vertical solid lines indicate the  $\eta_\gamma$  cut of eq. (25).

I for an integrated luminosity of  $2 \text{ fb}^{-1}$ . Statistical significance  $\sigma$  is defined by  $\sigma = S/\sqrt{B}$ , where  $S(B)$  is the number of signal (background) events after applying cuts and efficiency factors. A few comments are in order. First of all, the expected number of events diminishes for small  $h_f$  masses since fewer events pass the  $E_T^\gamma$  cut in eq. (25) as can be seen from Fig. 4. Secondly, the shape of the region presenting at least  $3\sigma$  ( $5\sigma$  or  $10\sigma$ ) significance in the large  $h_f$  mass region is the result of a competition between the phase space suppression of the cross section as  $m_{H^\pm}$  increases for fixed  $m_{h_f}$  and the growth of the  $H^\pm \rightarrow W^\pm h_f$  branching ratio; see Fig. 2. Furthermore, for a fixed number of events, the optimum reach in  $m_{H^\pm}$  takes place for  $m_{h_f} \simeq 30\text{--}40 \text{ GeV}$ . This is a consequence of the combined effects of cuts and phase space suppression as we have already discussed.

As one can see from the upper panel in Fig. 8, even in the low  $\tan\beta$  region the reach of the Tevatron RUN II is quite impressive in this scenario. If no events were observed above the backgrounds at RUN II, a large fraction of the  $m_{H^\pm} \otimes m_{h_f}$  plane would be excluded at the  $3\sigma$  level. The situation improves slightly for larger  $\tan\beta$  as can be seen from the lower panel of Fig. 8. Importantly, the expected number of events is rather large in the region  $m_{h_f} \lesssim 70 \text{ GeV}$  and  $m_{H^\pm} \lesssim 150 \text{ GeV}$ , such that it will be possible to reconstruct the  $h_f$  mass from the photon–photon invariant mass distribution; see Fig. 7.

For comparison, we present in Fig. 9 the expected signal significance of events containing three or more photons after cuts for the HTM. In our numerical analysis we take  $c_H = 1$  as a benchmark value, and the signal significance for other values of  $c_H$  can be obtained by simply rescaling the displayed numbers. From the bound  $s_H < 0.4$  one obtains  $c_H > 0.9$ . In the exact  $c_H = 1$  limit (i.e. triplet vev  $b = 0$ ) the neutrinos would not receive a mass at tree-level (see eq. 14). Extremely small  $s_H < 10^{-9}$  would require non-perturbative values of  $h_{ij}$  to generate realistic neutrino masses. We are interested in

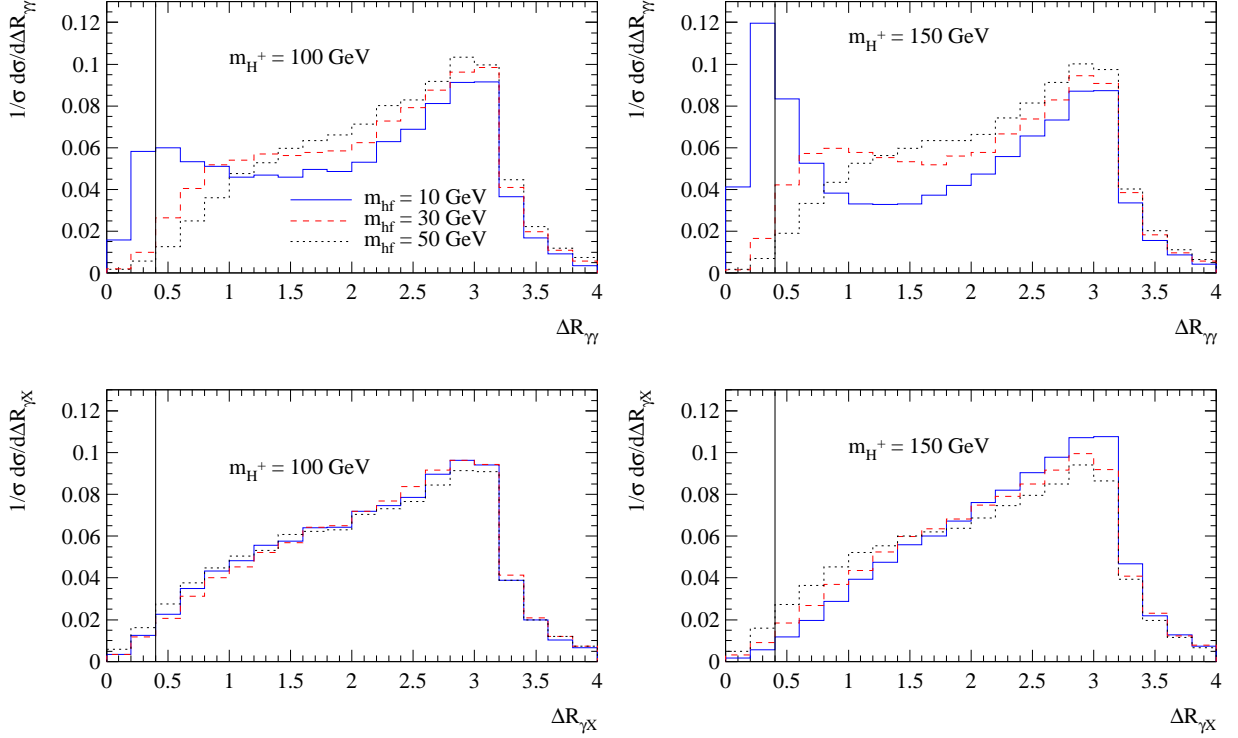


Figure 6: Normalized cone variable distributions between two photons (upper panels), a photon and a charged particle or jet (lower panels) for the same parameter used in Fig. 4. The vertical solid lines indicate the  $\Delta R$  cuts in eq. (26).

the interval  $0.9 < c_H < 0.99$  (corresponding to GeV scale triplet vev) in which  $H_1^{0'}$  decays primarily to photons in the detector, and neutrino mass is generated with a very small  $h_{ij} \sim 10^{-10}$ .

It is clear that a larger region of the  $m_{h_f} \otimes m_{H^\pm}$  parameter space can be probed in the HTM than in the 2HDM. In fact, at the  $3\sigma$  level RUN II will be able to exclude Higgs masses up to  $m_{H^\pm} \lesssim 240$  GeV or  $m_{h_f} \lesssim 100$  GeV. In order to understand the signal suppression if one requires an inclusive state containing four photons to pass our cuts, we present in Fig. 9 lower panel the expected number of events for the 2HDM, assuming  $\tan\beta = 30$  and an integrated luminosity of  $2 \text{ fb}^{-1}$ . As expected, not only the reach in  $m_{H^\pm}$  gets reduced to  $m_{H^\pm} \lesssim 150$  GeV at 95% C.L., but also the low and high  $h_f$  mass regions become substantially depleted.

## 5 Conclusions

Higgs bosons with very suppressed couplings to fermions ( $h_f$ ) can arise in various extensions of the Standard Model (SM) such as the Two Higgs Doublet Model (2HDM) Type I or Higgs Triplet Model (HTM). Their conventional production mechanism at hadron colliders  $qq' \rightarrow W^\pm h_f$  can be severely suppressed by either large  $\tan\beta$  or small triplet vacuum expectation value. In this scenario the complementary channel  $p\bar{p} \rightarrow H^\pm h_f$  is maximal and provides an alternative production mechanism. We studied the reaction  $qq' \rightarrow H^\pm h_f$  followed by the potentially important decay  $H^\pm \rightarrow h_f W^*$ . We performed a Monte Carlo simulation of the detection prospects for a light  $h_f$  where the branching ratio into photon pairs is dominant, which gives rise to multi-photon signatures with very low SM background. We showed that if a signal containing at least three photons is not seen at the Tevatron RUN II then a large portion of the  $m_{H^\pm}$  versus  $m_{h_f}$  plane can be excluded both in the small and large  $\tan\beta$  regimes of the 2HDM. Conversely, if a signal were observed then  $> 50$  events are expected for a light  $H^\pm$  and  $h_f$ , which would allow further detailed phenomenological studies.

## Acknowledgements

We would like to thank Oleksiy Atramentov for discussions concerning the SM backgrounds. This research was supported in part by Fundação de Amparo à Pesquisa do Estado de São Paulo (FAPESP), by Conselho Nacional de Desenvolvimento Científico e Tecnológico (CNPq), and by Conicyt grant No. 1040384.

## References

- [1] T. J. Weiler, *Proceedings of the 8th Vanderbilt Int. Conf. on High Energy Physics, Nashville, TN, Oct 8-10, 1987*; Edited by J. Brau and R. Panvini (World Scientific, Singapore, 1988), p219
- [2] H. E. Haber, G. L. Kane and T. Sterling, Nucl. Phys. B **161**, 493 (1979)
- [3] J. F. Gunion, H. E. Haber, G. L. Kane and S. Dawson, “The Higgs Hunter’s Guide,” (Reading, MA: Addison-Wesley, 1989)
- [4] H. Georgi and M. Machacek, Nucl. Phys. B **262**, 463 (1985); M. S. Chanowitz and M. Golden, Phys. Lett. B **165**, 105 (1985)
- [5] A. Stange, W. J. Marciano and S. Willenbrock, Phys. Rev. D **49**, 1354 (1994)
- [6] M. A. Diaz and T. J. Weiler, arXiv:hep-ph/9401259
- [7] V. D. Barger, N. G. Deshpande, J. L. Hewett and T. G. Rizzo, arXiv:hep-ph/9211234. In Argonne 1993, Physics at current accelerators and supercolliders\* 437-442

- [8] H. Pois, T. J. Weiler and T. C. Yuan, Phys. Rev. D **47**, 3886 (1993)
- [9] A. G. Akeroyd, Phys. Lett. B **368**, 89 (1996)
- [10] A. Barroso, L. Brucher and R. Santos, Phys. Rev. D **60**, 035005 (1999)
- [11] L. Brucher and R. Santos, Eur. Phys. J. C **12**, 87 (2000)
- [12] G. Abbiendi *et al.* [OPAL Collaboration], Phys. Lett. B **544**, 44 (2002)
- [13] P. Abreu *et al.* [DELPHI Collaboration], Phys. Lett. B **507**, 89 (2001); Eur. Phys. J. C **35**, 313 (2004)
- [14] A. Heister *et al.* [ALEPH Collaboration], Phys. Lett. B **544**, 16 (2002)
- [15] P. Achard *et al.* [L3 Collaboration], Phys. Lett. B **534**, 28 (2002); Phys. Lett. B **568**, 191 (2003).
- [16] B. Abbott *et al.* [DØ Collaboration], Phys. Rev. Lett. **82**, 2244 (1999)
- [17] T. Affolder *et al.* [CDF Collaboration], Phys. Rev. D **64**, 092002 (2001)
- [18] S. Mrenna and J. Wells, Phys. Rev. D **63**, 015006 (2001)
- [19] V. M. Abazov *et al.* [D0 Collaboration], arXiv:hep-ex/0508054.
- [20] G. Landsberg and K. T. Matchev, Phys. Rev. D **62**, 035004 (2000)
- [21] A. Melnitchouk [D0 Collaboration], Int. J. Mod. Phys. A **20**, 3305 (2005)
- [22] A. G. Akeroyd and M. A. Diaz, Phys. Rev. D **67**, 095007 (2003)
- [23] A. G. Akeroyd, M. A. Diaz and F. J. Pacheco, Phys. Rev. D **70**, 075002 (2004)
- [24] A. G. Akeroyd, Nucl. Phys. B **544**, 557 (1999)
- [25] A. G. Akeroyd, Phys. Lett. B **442**, 335 (1998)
- [26] J. F. Gunion and H. E. Haber, arXiv:hep-ph/0506227.
- [27] J. Schechter and J. W. F. Valle, Phys. Rev. D **22**, 2227 (1980).
- [28] F. Cuyppers and S. Davidson, Eur. Phys. J. C **2**, 503 (1998); Y. Kuno and Y. Okada, Rev. Mod. Phys. **73**, 151 (2001)
- [29] J. F. Gunion, R. Vega and J. Wudka, Phys. Rev. D **42**, 1673 (1990)
- [30] A. Kundu and B. Mukhopadhyaya, Int. J. Mod. Phys. A **11**, 5221 (1996); H. E. Haber and H. E. Logan, Phys. Rev. D **62**, 015011 (2000)
- [31] A. G. Akeroyd, Phys. Lett. B **353**, 519 (1995).

- [32] P. Bamert and Z. Kunszt, Phys. Lett. B **306**, 335 (1993)
- [33] J. F. Gunion, R. Vega and J. Wudka, Phys. Rev. D **43**, 2322 (1991).
- [34] A. Alves and T. Plehn, Phys. Rev. D **71**, 115014 (2005).
- [35] F. Maltoni and T. Stelzer, JHEP **0302**, 027 (2003); T. Stelzer and W.F. Long, Phys. Commun. **81**, 357 (1994).
- [36] J. Pumplin, D.R. Stump, J. Huston, H.L. Lai, P. Nadolsky, W.K. Tung, JHEP **0207**, 012 (2002).
- [37] S. Dawson, S. Dittmaier and M. Spira, Phys. Rev. D **58**, 115012 (1998)
- [38] A. Gajjar [CDF Collaboration], arXiv:hep-ex/0505046; V. M. Abazov *et al.* [D0 Collaboration], Phys. Rev. D **71**, 091108 (2005) A. Melnitchouk, Ph.D. Thesis, FERMILAB-THESIS-2003-23 (2003).

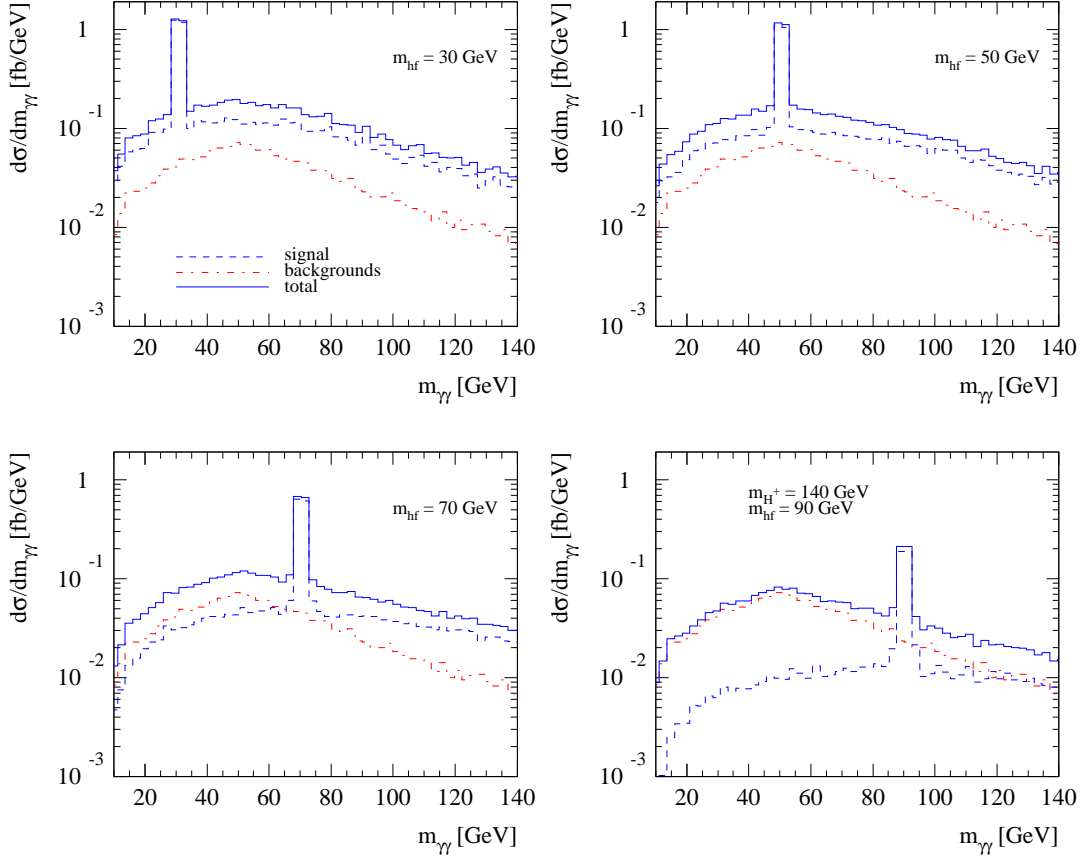


Figure 7: The photon–photon invariant mass spectrum for  $m_{H^\pm} = 150$  GeV,  $m_{h_f} = 30$ , 50, 70 GeV, and  $m_{H^\pm} = 140$  GeV,  $m_{h_f} = 90$  GeV at the upper left, upper right, bottom left, and bottom right panels, respectively. Also shown are the sum of all backgrounds consisting of  $3\gamma + X$  final states. In these plot we entered the invariant mass of all photon pair possible combinations. In all cases we set  $\tan\beta = 30$ .

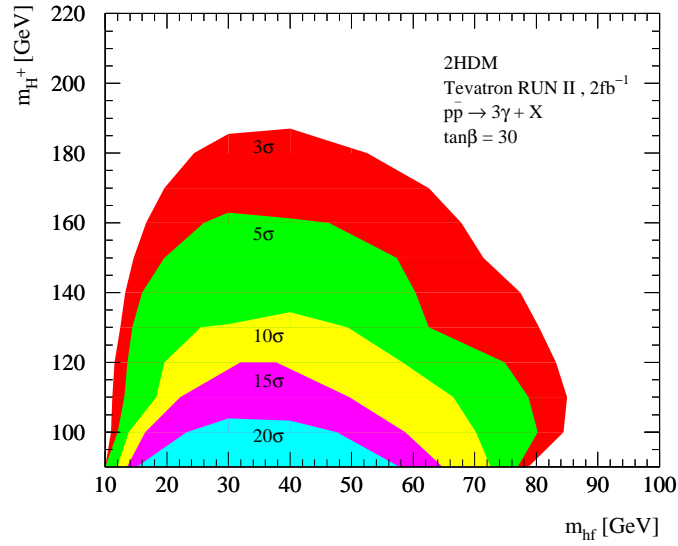
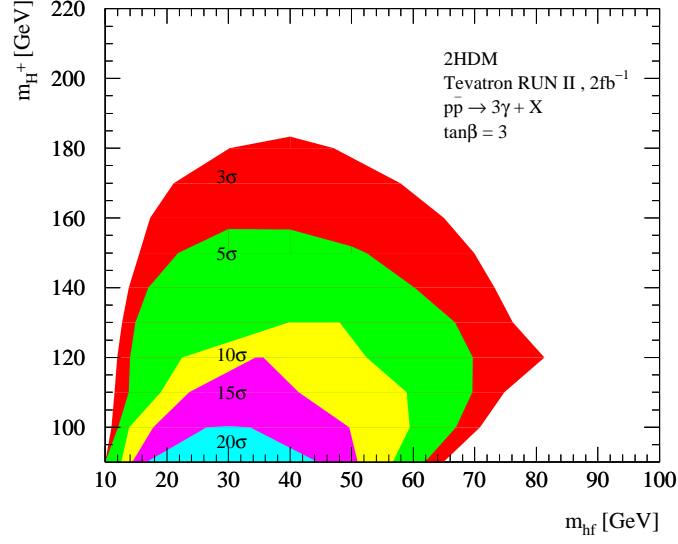


Figure 8: Expected signal statistical significance presenting three or more photons in the  $m_{H^\pm} \otimes m_{h_f}$  plane assuming an integrated luminosity of  $2 \text{ fb}^{-1}$  at the Tevatron RUN II. We assumed the 2HDM Model I and took  $\tan \beta = 3$  (30) in the upper (lower) panel.

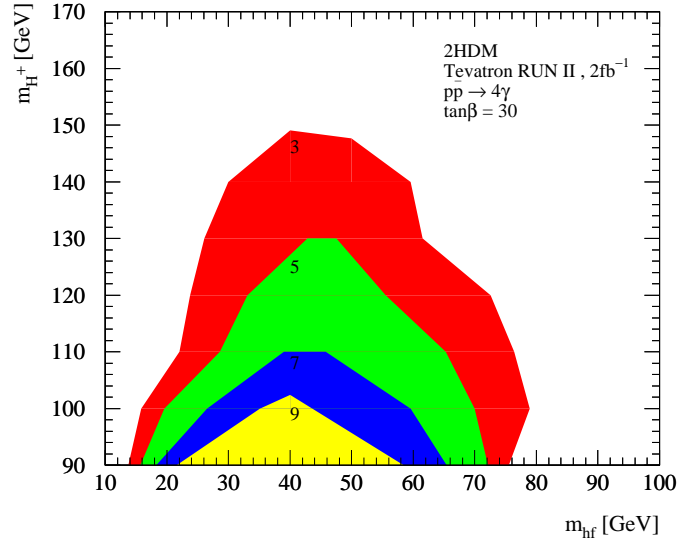
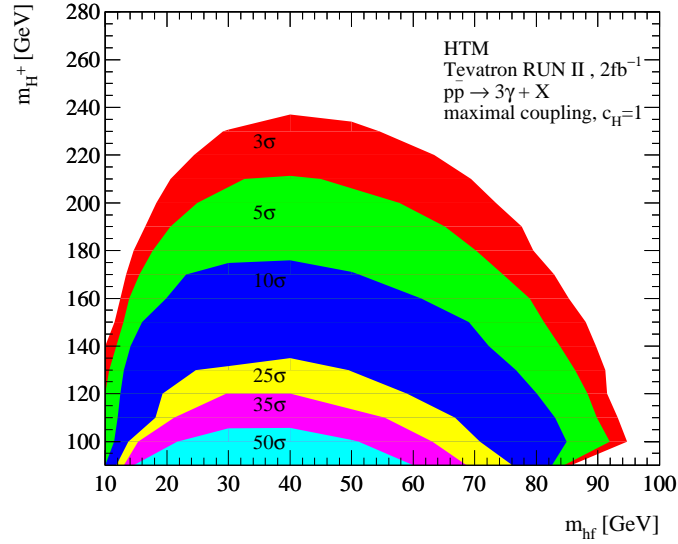


Figure 9: In the upper panel we display the expected signal statistical significance containing three or more photons in the  $m_{H^\pm} \otimes m_{h_f}$  plane in the HTM framework, assuming an integrated luminosity of  $2\text{fb}^{-1}$  at the Tevatron RUN II. In the lower panel we present the expected number of events presenting four photons in the  $m_{H^\pm} \otimes m_{h_f}$  plane for the 2HDM Model I and assuming  $\tan\beta = 30$ .